Ultra-low mode volume on-substrate silicon nanobeam cavity

JUN ZHOU,[1,3] **JIAJIU ZHENG,**[2] (iD) **ZHUORAN FANG,**[2] **PEIPENG XU,**[1,3,5] (iD) **AND ARKA MAJUMDAR**[2,4,6] (iD)

[1]*Laboratory of Infrared Materials and Devices, Advanced Technology Research Institute, Ningbo University, Ningbo 315211, China*
[2]*Department of Electrical and Computer Engineering, University of Washington, Seattle, WA 98195, USA*
[3]*Key Laboratory of Photoelectric Detection Materials and Devices of Zhejiang Province, Ningbo, 315211, China*
[4]*Department of Physics, University of Washington, Seattle, WA 98195, USA*
[5]*xupeipeng@nbu.edu.cn*
[6]*arka@uw.edu*

Abstract: We design and fabricate an on-substrate bowtie photonic crystal (PhC) cavity in silicon. By optimizing the bowtie shapes in the unit cells of the PhC cavity, the maximum of the electric field can be highly confined in the bowtie tips. Due to such confinement, an ultra-low mode volume of $\sim 0.1(\lambda/n_{\mathrm{Si}})^3$ is achieved, which is more than an order of magnitude smaller than the previous on-substrate nanobeam cavities. An ultra-high quality (Q) factor as large as 10^6 is predicted by simulation, and up to 1.4×10^4 is measured in experiment. The observation of pronounced thermo-optic bistability is consistent with the strong confinement of light in the cavities.

1. Introduction

Optical cavities are able to trap light at discrete resonant frequencies in a tiny volume [1], in which the interaction of light with matter can be dramatically enhanced via temporal and spatial confinement of light. Quality (Q) factor and effective mode volume (V_m), two figures of merit in optical cavities, are of great importance in the enhancement of light-matter interaction. The Q factor describes the temporal confinement of the cavity mode, which is proportional to the cavity photon lifetime. The mode volume represents the spatial confinement and refers to the capability to confine light into a closely confined space, which quantifies the electric field strength per photon. The mode volume of a dielectric cavity [described by the spatially varying permittivity $\varepsilon(r)$] is given by the ratio of the total electric energy to the maximum electric energy density:

$$V_{\mathrm{m}} = \frac{\int \varepsilon(\vec{r})|E(\vec{r})|^2 dV}{\max(\varepsilon(\vec{r})|E(\vec{r})|^2)}, \tag{1}$$

The long photon lifetime and strong light confinement in these optical cavities have led to many fundamental studies of optical physics at nanoscale and integrated photonic applications, including, ultralow threshold lasers [2,3], faster and low power optical data processing [4], enhanced nonlinear process [5], strong coupling with quantum emitters [6,7], and optical sensors with ultralow detection limit [8,9].

To pursue a large quality factor to modal volume ratios (Q/V_{m}), various types of optical cavities have been reported, including microring [10], microdisk [11], and one-dimensional (1D) or two-dimensional (2D) photonic crystal (PhC) cavities [12–14]. Among them, 1D PhC nanobeam cavities offer exceptional Q/V_{m} as well as relative ease of design, and fabrication, which make them an attractive alternative to 2D PhC cavities. Typical PhC nanobeam cavities exploit a simple unit cell geometry, such as circles, ellipses or rectangles [12,15–17], which

when properly designed can reduce the effective mode volume roughly to unity, i.e., to the scale of $(\lambda/n_{Si})^3$. To further squeeze light into the nanoscale region, a primary strategy is to introduce an abrupt index discontinuity along the electric field polarization direction, which not only increases the maximum field intensity but also confines the maximum field to a region of lower refractive index. Confining light to lower index (often air) can be beneficial for application involving optical sensing, or hybrid integrated photonics, where the new material is introduced in the space where there was air before. Slotted photonic crystal cavities [18–20] reduce the V_m to ~0.01 $(\lambda/n_{air})^3$, almost one orders of magnitude smaller than traditional photonic crystal cavities. However, without any further design tailoring and parameter optimization, introducing an air slot can presumably reduce the quality factor by over several orders of magnitude [18]. Also, slotted photonic crystal structures inherently confine resonant modes within a low-index region. Thus, they are not suitable for the applications requiring strong light-matter interaction in higher refractive index materials, such as silicon, silicon carbide, silicon nitride, and other highly nonlinear optically active materials. Recently, PhC cavities with bowtie shapes designed by self-similar design have been demonstrated and extremely light concentration can be achieved [21,22]. Suspended bowtie photonic crystal cavities were also experimentally demonstrated recently [23]. However, suspending the PhC cavity off the substrate and v-groove etching are required, which is not mechanically robust [24] and requires challenging fabrication.

In this paper, we describe an on-substrate bowtie PhC nanobeam microcavity with ultra-small mode volume. Employing three-dimensional finite-difference-time-domain (3D-FDTD) and finite-element method (FEM) simulations, a mode volume V_m (~0.1$(\lambda/n_{Si})^3$) can be achieved while maintaining a high Q-factor of $>1\times10^6$ by tapering the bowtie shapes. By fabricating a series of such devices, we experimentally demonstrated a Q factor of ~1.4$\times10^4$.

2. Design and analysis

Figure 1(a) presents the schematic of a bowtie PhC nanobeam cavity. The Silicon-on-Insulator (SOI) wafer with 220 nm thick top Si device layer on a 3-μm-thick silica insulation layer has been employed in our work. The refractive index of the silica buffer and the silicon core layer are taken as 1.44 and 3.46, respectively. The upper cladding is set to be air with a refractive index of 1.0. The proposed PhC nanobeam cavity comprises a sequence of bowtie-shape unit cells, forming the Gaussian mirrors on either side. From the top view of the bowtie PhC cavity, shown in Fig. 1(b), the transverse (x-axis) tip width is W_c, and the longitudinal (y-axis) heights of each unit cell are W_h and W_b, respectively. The inset shows an enlarged view of the black framed part. To minimize scattering loss in the propagation direction x, we keep the period a, i.e., the transverse (x-axis) distance between the bowtie, constant to ensure optical phase matching between adjacent unit cells [25]. To create the cavity mode, the widths of bowtie shapes are modulated from $W_x(0)$ in the center to $W_x(i_{max})$ on the each sides parabolically: $W_x(i)=W_x(0) +(i-1)^2\times(W_x(i_{max})-W_x(0))/(i_{max}-1)^2$, i increases from 1 to i_{max}. The bowtie PhC cavity was designed using the 3D-FDTD approach and FEM for simulations of photonic band structure and electric field distribution, respectively. Figures 1(c)–(d) show the electric field distribution of the bowtie PhC cavity at resonance wavelength from the top view in the xy plane and xz plane, respectively. The simulations reveal that the fundamental resonance mode exhibits the desired Gaussian shaped profile with the maximal field strength at the center of the cavity. In this simulation, there are 30 bowtie-shaped unit cells in the taper region on each side of the PhC cavity, and only partial cells are shown in the figures. The TE-polarized band diagrams of the periodic bowtie cells simulated with Bloch boundary conditions with width $W_x(0) = 0.6a$ (width of the center bowtie) and $W_x(i_{max}) = 0.84a$ (width of the edge bowtie) are given in Fig. 1(e). The resonance frequency of the cavity mode [the dot and dashed line in Fig. 1(e)] is slightly lower than the dielectric band edge of the bowtie cell with $W_x(0) = 0.6a$, which is consistent with the perturbation theory described by Quan et al. [25]. Here, the

period length is chosen to be $a = 444$ nm to ensure the resonant wavelength of the fundamental mode is around telecommunication wavelength range. Figures 1(f) and 1(g) show the top and cross-section view of the electric field distribution of lower band-edge mode in the center unit cell and it can be found that most of the electric field of the resonant mode is highly confined between the bowtie tips.
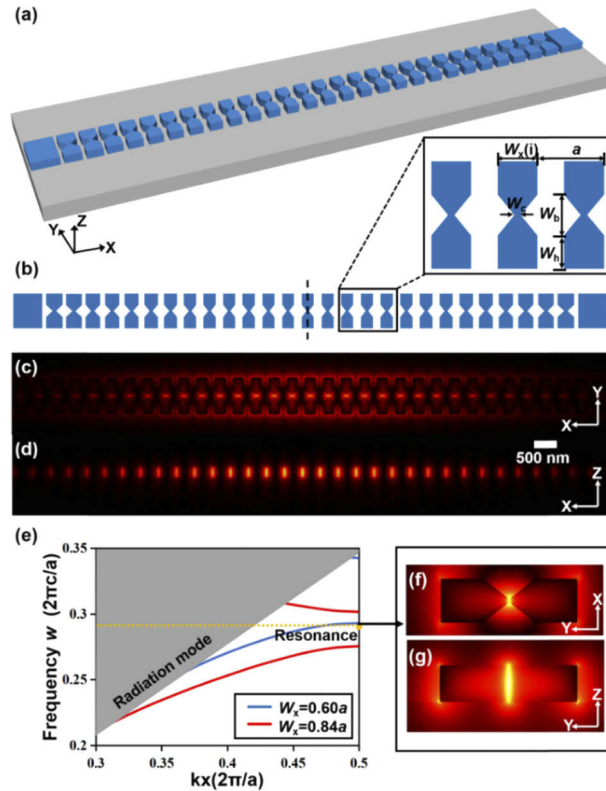
Fig. 1. (a) Schematic of the bowtie PhC cavity in silicon-on-insulator platform. (b) Top view of the bowtie PhC cavity. Inset: enlarged view of the framed part. The electric field distribution at the resonance wavelength (c) in the *xy* plane and (d) in the *xz* plane. (e)The blue line ($W_x = 0.6a$) and red lines ($W_x = 0.84a$) show the band diagram of the bowtie PhC cavity. The yellow dashed line indicates the resonant frequency. The gray region indicates the light cone of the silica. The corresponding field distributions of lower band-edge mode in the center unit cell at the (f) top view (*xy* plane) and (g) cross-sectional view (*yz* plane).

To further optimize the performance of the bowtie PhC cavity, we have investigated the effect of tip width W_c on the Q factor and V_m. Figure 2(a) shows that low mode volumes are obtained when W_c is small, and the mode volume decreases approximately linearly with the decrease of W_c. This can be easily understood that the smaller tip width of the bowtie shape can significantly increase the electric energy density and correspondingly shrink the mode volume. Considering the trade-off between the device performance and ease of fabrication, the width W_c is chosen to be 20 nm. Figure 2(b) shows the relationship between the mode volume and the width of $W_x(0)$. We can find that the mode volume of the bowtie PhC cavity is within the range of 0.1~0.13 $(\lambda/n_{Si})^3$, while the Q factor is in the range of $5.7 \times 10^5 \sim 1.05 \times 10^6$, indicating that the mode volume and Q factor are only weakly dependent on $W_x(0)$.

Figure 2(c) shows the mode volume and Q factor of the bowtie PhC cavity with different W_b. We can find that the Q factor increases slightly with the increase of width W_b, while the mode
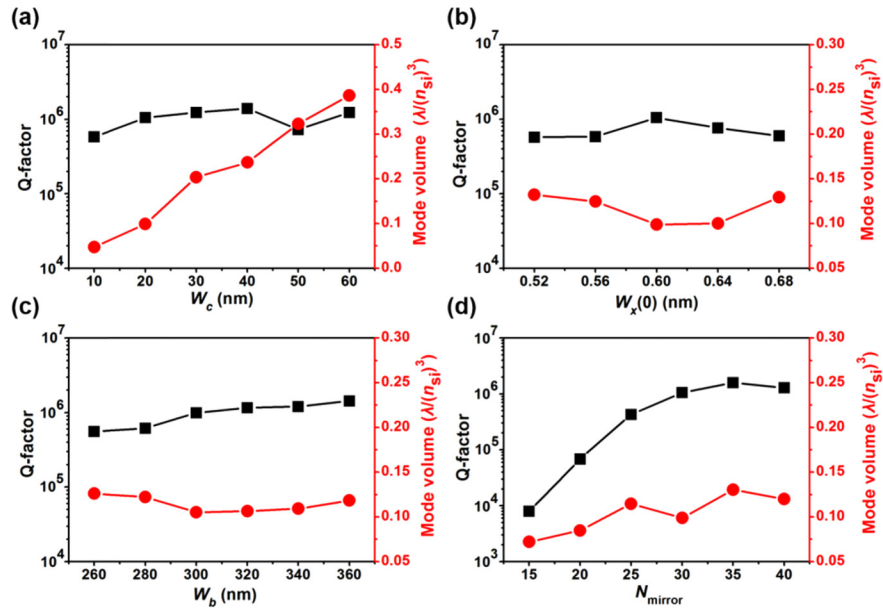
Fig. 2. The variation of the Q factor and the mode volume of the bowtie PhC with a change in the (a) tip width of the W_c, (b) width $W_x(0)$ of the bowtie-shaped unit cell, (c) W_b, and (d) number of the Gaussian mirror (N_{mirror}).

volume remains almost unchanged. For the present cavity, the number of the Gaussian mirrors (N_{mirror}) on both sides of the cavity can also affect the Q factor and mode volume, as shown in Fig. 2(d). The Q factor of the PhC cavity rises rapidly with the increase of N_{mirror} till $N_{mirror} = 30$ and then stays at high values. This is because $N_{mirror} = 30$ is large enough for the PhC cavity to support the well-confined resonant optical mode. In contrast, the mode volume of the bowtie PhC cavity increases slightly in the range of 0.07~0.13 $(\lambda/n_{Si})^3$. This can be explained by the fact that the Gaussian field permeates into the side mirror with the increase of the N_{mirror}.

From the above optimization and analysis, the geometric parameters of the bowtie PhC nanobeam cavity are summarized to be: $a = 444$ nm, $W_c = 20$ nm, $W_x(0) = 0.6a$, $W_x(i_{max}) = 0.84a$, $W_b = 314$ nm, $W_h = 252$ nm, and $N_{mirror} = 30$ on both sides. With these parameters, most of the electric field of resonant mode is confined between the bowtie tips of the PhC cavity. Thus, both ultra-high Q factor (more than 1×10^6) and ultra-small mode volume ($\sim 0.1(\lambda/n_{Si})^3$) can be achieved. This mode volume is about one order of magnitude smaller than that of previous non-suspended PhC microcavities [13,17,26]. The resonant wavelength of the fundamental mode used for the cavities is 1527.8 nm.

3. Fabrication and measurement

Our devices were fabricated from silicon-on-insulator (SOI) wafers with a ~220 nm thick Si device layer and a 3-μm-thick buried oxide. The cavity pattern was defined by direct-writing 100 keV acceleration voltage electron-beam lithography (JEOL JBX-6300FS) utilizing a positive tone electron beam resist (ZEP-520A) and transferred onto the underlying silicon core layer by an anisotropic inductively coupled plasma (ICP) process using a gas mixture of SF_6 and C_4F_8. Figures 3(a) and 3(b) show the scanning electron micrographs (SEMs) of the fabricated cavity, which is formed utilizing a pair of modulated mirrors, consisting of $N_{mirror}=30$ mirror segments. On either side of the modulated mirror, a 10-μm-length input/output tapers waveguides are used to connect each device and the standard 500-nm-width Si waveguide with a length of several

hundred microns, at the ends of which focusing TE-type grating couplers (GCs) are located to enable local testing of the devices. Figure 3(c) shows the fully etched transverse electric (TE) type focusing sub-wavelength grating coupler (GC) with a period of 593 nm, and which are designed for a negative angle (-31°). The polarization of the input light was controlled to match the fundamental quasi-TE mode of the waveguide by a manual fiber polarization controller (Thorlabs FPC526). The straight single-mode waveguides with the same grating couplers were also fabricated on the same chip to normalize the spectra. A tunable telecom laser source (Santec TSL-510) with a wavelength ranging from 1425 to 1565 nm and a high-resolution and sensitivity power meter (Keysight 81634B) as the detector were used to measure the performance of the fabricated cavities. Figure 3(d) shows the optical transmission spectrum of the bowtie PhC cavity normalized by the peak resonance transmission. The cavity has a fundamental mode resonance at 1525.8 nm. Lorentzian fitting of the fundamental mode resonance reveals the full width at half maximum (FWHM) is approximately equal 108 pm, indicating that the measured quality factor is more than 1.4×10^4. The extinction ratio is larger than 21 dB. The quality factor and the extinction ratio are smaller than the simulated values due to fabrication imperfections and material loss. In addition, we did find the bowtie PhC cavity supports the higher order resonance mode, which can be well separated since the Q factor of high-order modes is much smaller than the fundamental one. Further optimization of the fabrication parameters may lead to bowtie PhC cavities with an even higher Q factor.
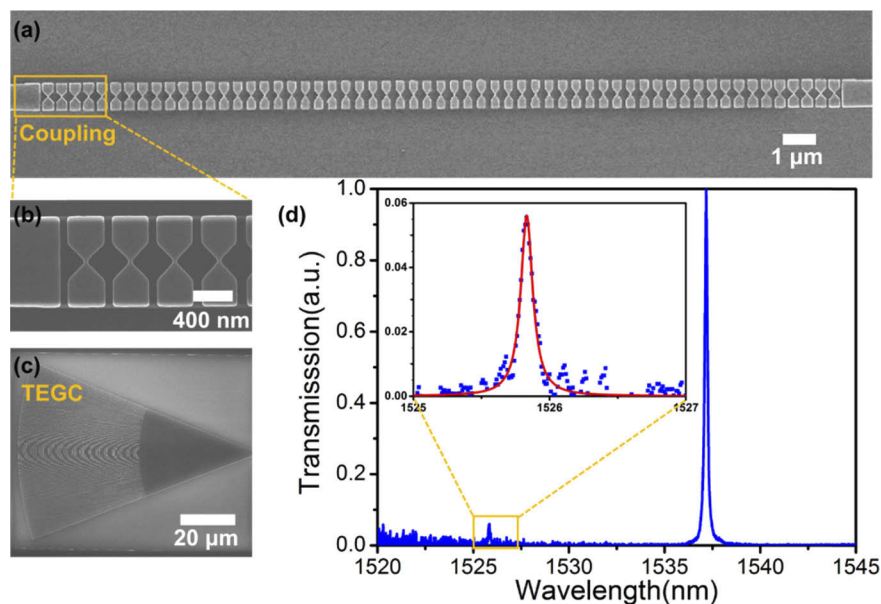
Fig. 3. (a), (b) The SEM of all device and the coupling region connecting the strip/bowtie structure waveguides. (c) SEM of the GC. (d) The measured transmission spectrum of the bowtie PhC cavity in air. The fundamental mode has a Q factor of 1.4×10^4 at $\lambda = 1525.8$ nm.

To demonstrate the ultra-small mode volume in the bowtie PhC cavities, we performed an optical bistability measurement of the cavity. Optical bistability due to the thermo-optic effect (i.e., change of refractive index due to heat) has been widely observed in silicon cavities [13,27]. Silicon has a positive thermo-optic coefficient causing the resonance wavelength of the cavity to red-shift with increasing power, as shown in Fig. 4(a). We estimated the power incident on the device using the coupling efficiency deduced from transmission of the straight waveguide without a cavity. Due to both high Q and the small V_m, we were able to observe optical bistability

at remarkably low intensities in our nanobeam cavity. When the input optical power increases from 0.59 µW to 29.41 µW, the transmission spectrum changes from a Lorentzian shape to a slant Lorentzian shape, while the overall resonance wavelength shifts towards the red by about 80 pm. The slant Lorentzian shape originates from the thermo-optic nonlinearity coming from the photothermal heating; the total red-shift is a typical characteristic of such thermo-optic effect. The thermo-optic effect is mainly caused by linear absorption as well as some nonlinear processes due to the large circulating intensity in the cavity, such as two-photon and free-carrier absorption as well as plasma and Kerr dispersion [28]. V. R. Almeida et al. [29] found that the nonlinear absorption coefficient in cavity is much lower than its linear counterpart and suggests that the underlying physical process is indeed primarily linear. As the power in the output waveguide (P_{out}) is proportional to the energy in the cavity, we can write $P_b \approx (P_{out}/\Delta\lambda)\Gamma$ [30], where P_b is the characteristic power to observe bistability [31], namely the output power when the resonance has been shifted by its linewidth and 2Γ is the FWHM of the resonance. Fitting the resonance wavelengths as the function of the measured output power, we can obtain the resonance-wavelength shift $\Delta\lambda$ as the output power P_{out} increases [see Fig. 4(b)]. Using 2Γ as the cavity linewidth measured at low laser power (108 pm), we can write $P_{out}/\Delta\lambda = -1/3.19$ nW/pm and thus $P_b = \sim17$ nW. This power level is much lower than other photonic crystal systems [13,32]. We attribute this low power to observe the nonlinear optical effects to the ultra-low mode volume of the bowtie cavity.
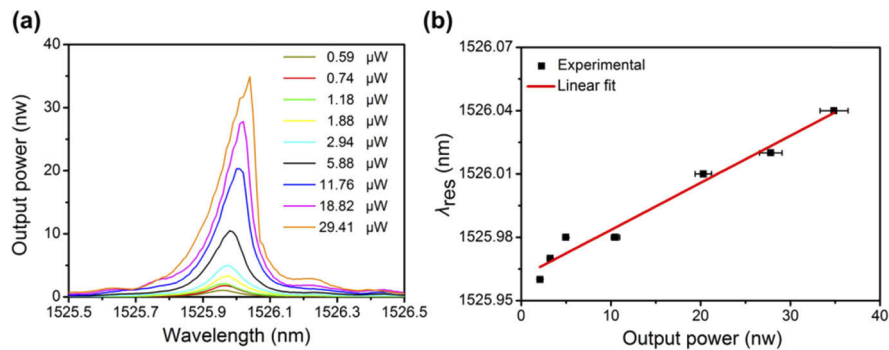
Fig. 4. (a) Asymmetric transmission spectra of the bowtie PhC single nanobeam cavity resonant mode at different input powers, showing optical bistability. The laser wavelength was swept from shorter to longer wavelengths across the cavity resonance. (b) Resonance-wavelength λ_{res} as a functin of the output power.

To further investigate the effect of temperature on the resonant wavelength of the bowtie PhC cavity, we heat the entire cavity. During the optical measurement, a thermoelectric controller (TEC, TE Technology TC-720) is used to control the temperature of the cavity. The power of the coupled light was selected to be low enough (0.59 µW) to minimize the thermal-optic effects of the silicon [29]. Figure 5(a) shows the measured transmission spectra of the fabricated bowtie PhC cavity with the ambient temperature changing from 20 °C to 45 °C with a step of 5 °C. From this figure, we can find that with the increasing of the ambient temperature, there is a red-shift of the resonant wavelength for the bowtie PhC cavity. Figure 5(b) shows that the wavelength drift induced by temperature is linear, indicating a red shift of approximately 41.3 pm when the ambient temperature is increased by 1°C. The pink line indicates the error estimates with 95% prediction interval. Using the known thermo-optic coefficients dn/dT for silicon (1×10^{-5} K^{-1}), and silica (1.86×10^{-4} K^{-1}), and assuming that thermo-optic coefficients of air can be neglected (the dn/dT for air is -9.4×10^{-7} K^{-1}), we find the resonant wavelength dependent on temperature is ~45 pm/°C, which is in rough agreement with the measured values.
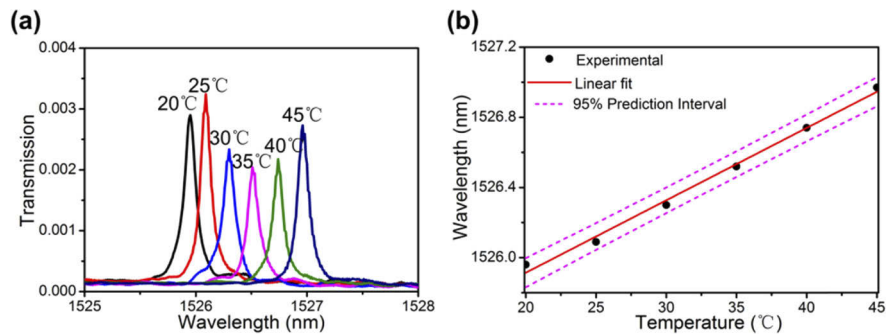
Fig. 5. (a) Transmission spectrum of the fabricated bowtie PhC single nanobeam cavity at different ambient temperatures. (b) Resonant wavelength varies with the ambient temperature for the bowtie PhC nanobeam cavity. The pink line indicates the error estimates with 95% prediction interval.

4. Summary

We have demonstrated an on-substrate bowtie PhC nanobeam cavity in silicon. The bowtie geometry is utilized to offer strong confinement and localized field enhancements, therefore resulting in an ultra-small mode volume of $\sim0.1(\lambda/n_{Si})^3$. Benefitting from the Gaussian-shaped field profile within the cavity, an optimized Q factor of 1×10^6 in simulations and 1.4×10^4 in fabricated devices has been achieved. Furthermore, the total size for the bowtie PhC cavity is only 26.2 μm×0.8 μm. The observation of significant thermo-optic bistability is consistent with the high Q factor and low mode volume in the bowtie PhC cavity. The availability of such compact, high Q and ultrasmall V_m nanobeam cavity makes them excellent candidates to hybridize with optically active materials on the tips (which is the case for many polymers, oxides and liquid solvents), where the electric field has its maximum, and could be used in various applications including nonlinear optics, quantum optics, ultra-sensitive single atom detection, optical switches, optical sensor, optical modulators and low threshold lasers.

References

1. K. J. Vahala, "Optical microcavities," Nature **424**(6950), 839–846 (2003).
2. S. Matsuo, A. Shinya, T. Kakitsuka, K. Nozaki, T. Segawa, T. Sato, Y. Kawaguchi, and M. Notomi, "High-speed ultracompact buried heterostructure photonic-crystal laser with 13 fJ of energy consumed per bit transmitted," Nat. Photonics **4**(9), 648–654 (2010).

3. S. Wu, S. Buckley, J. R. Schaibley, L. Feng, J. Yan, D. G. Mandrus, F. Hatami, W. Yao, J. Vučković, A. Majumdar, and X. Xu, "Monolayer semiconductor nanocavity lasers with ultralow thresholds," Nature **520**(7545), 69–72 (2015).

4. K. Nozaki, T. Tanabe, A. Shinya, S. Matsuo, T. Sato, H. Taniyama, and M. Notomi, "Sub-femtojoule all-optical switching using a photonic-crystal nanocavity," Nat. Photonics **4**(7), 477–483 (2010).

5. M. SoljaČiĆ and J. D. Joannopoulos, "Enhancement of nonlinear effects using photonic crystals," Nat. Materials **3**(4), 211–219 (2004).

6. D. Englund, A. Majumdar, M. Bajcsy, A. Faraon, P. Petroff, and J. Vučković, "Ultrafast Photon-Photon Interaction in a Strongly Coupled Quantum Dot-Cavity System," Phys. Rev. Lett. **108**(9), 093604 (2012).

7. S. Sun, H. Kim, Z. Luo, G. S. Solomon, and E. Waks, "A single-photon switch and transistor enabled by a solid-state quantum memory," Science **361**(6397), 57–60 (2018).

8. A. M. Armani, R. P. Kulkarni, S. E. Fraser, R. C. Flagan, and K. J. Vahala, "Label-Free, Single-Molecule Detection with Optical Microcavities," Science **317**(5839), 783–787 (2007).

9. P. Xu, J. Zheng, J. Zhou, Y. Chen, C. Zou, and A. Majumdar, "Multi-slot photonic crystal cavities for high-sensitivity refractive index sensing," Opt. Express **27**(3), 3609–3616 (2019).

10. W. Bogaerts, P. De Heyn, T. Van Vaerenbergh, K. De Vos, S. Kumar Selvaraja, T. Claes, P. Dumon, P. Bienstman, D. Van Thourhout, and R. Baets, "Silicon microring resonators," Laser Photonics Rev. **6**(1), 47–73 (2012).

11. M. Soltani, S. Yegnanarayanan, and A. Adibi, "Ultra-high Q planar silicon microdisk resonators for chip-scale silicon photonics," Opt. Express **15**(8), 4694–4704 (2007).

12. E. Kuramochi, H. Taniyama, T. Tanabe, K. Kawasaki, Y.-G. Roh, and M. Notomi, "Ultrahigh-Q one-dimensional photonic crystal nanocavities with modulated mode-gap barriers on SiO2 claddings and on air claddings," Opt. Express **18**(15), 15859–15869 (2010).

13. Q. Quan, P. B. Deotare, and M. Loncar, "Photonic crystal nanobeam cavity strongly coupled to the feeding waveguide," Appl. Phys. Lett. **96**(20), 203102 (2010).

14. Y. Akahane, T. Asano, B.-S. Song, and S. Noda, "High-Q photonic nanocavity in a two-dimensional photonic crystal," Nature **425**(6961), 944–947 (2003).

15. P. B. Deotare, M. W. McCutcheon, I. W. Frank, M. Khan, and M. Loncar, "High quality factor photonic crystal nanobeam cavities," Appl. Phys. Lett. **94**(12), 121106 (2009).

16. Q. Quan, I. B. Burgess, S. K. Y. Tang, D. L. Floyd, and M. Loncar, "High-Q, low index-contrast polymeric photonic crystal nanobeam cavities," Opt. Express **19**(22), 22191–22197 (2011).

17. A. R. M. Zain, N. P. Johnson, M. Sorel, and R. M. De la Rue, "Ultra high quality factor one dimensional photonic crystal/photonic wire micro-cavities in silicon-on-insulator (SOI)," Opt. Express **16**(16), 12084–12089 (2008).

18. J. D. Ryckman and S. M. Weiss, "Low mode volume slotted photonic crystal single nanobeam cavity," Appl. Phys. Lett. **101**(7), 071104 (2012).

19. P. Seidler, K. Lister, U. Drechsler, J. Hofrichter, and T. Stoeferle, "Slotted photonic crystal nanobeam cavity with an ultrahigh quality factor-to-mode volume ratio," Opt. Express **21**(26), 32468–32483 (2013).

20. A. Gondarenko and M. Lipson, "Low modal volume dipole-like dielectric slab resonator," Opt. Express **16**(22), 17689–17694 (2008).

21. S. Hu and S. M. Weiss, "Design of Photonic Crystal Cavities for Extreme Light Concentration," ACS Photonics **3**(9), 1647–1653 (2016).

22. H. Choi, M. Heuck, and D. Englund, "Self-Similar Nanocavity Design with Ultrasmall Mode Volume for Single-Photon Nonlinearities," Phys. Rev. Lett. **118**(22), 223605 (2017).

23. S. Hu, M. Khater, R. Salas-Montiel, E. Kratschmer, S. Engelmann, W. M. J. Green, and S. M. Weiss, "Experimental realization of deep-subwavelength confinement in dielectric optical resonators," Sci. Adv. **4**(8), eaat2355 (2018).

24. T. K. Fryett, Y. Chen, J. Whitehead, Z. M. Peycke, X. Xu, and A. Majumdar, "Encapsulated Silicon Nitride Nanobeam Cavity for Hybrid Nanophotonics," ACS Photonics **5**(6), 2176–2181 (2018).

25. Q. Quan and M. Loncar, "Deterministic design of wavelength scale, ultra-high Q photonic crystal nanobeam cavities," Opt. Express **19**(19), 18529–18542 (2011).

26. Y. Zhang, S. Han, S. Zhang, P. Liu, and Y. Shi, "High-Q and High-Sensitivity Photonic Crystal Cavity Sensor," IEEE Photonics J. **7**(5), 1–6 (2015).

27. L.-D. Haret, T. Tanabe, E. Kuramochi, and M. Notomi, "Extremely low power optical bistability in silicon demonstrated using 1D photonic crystal nanocavity," Opt. Express **17**(23), 21108–21117 (2009).

28. T. Uesugi, B.-S. Song, T. Asano, and S. Noda, "Investigation of optical nonlinearities in an ultra-high-Q Si nanocavity in a two-dimensional photonic crystal slab," Opt. Express **14**(1), 377–386 (2006).

29. V. R. Almeida and M. Lipson, "Optical bistability on a silicon chip," Opt. Lett. **29**(20), 2387–2389 (2004).

30. L. Jin, X. Fu, B. Yang, Y. Shi, and D. Dai, "Optical bistability in a high-Q racetrack resonator based on small SU-8 ridge waveguides," Opt. Lett. **38**(12), 2134–2136 (2013).

31. J. Bravo-Abad, A. Rodriguez, P. Bermel, S. G. Johnson, J. D. Joannopoulos, and M. Soljačić, "Enhanced nonlinear optics in photonic-crystal microcavities," Opt. Express **15**(24), 16161–16176 (2007).

32. M. Notomi, A. Shinya, S. Mitsugi, G. Kira, E. Kuramochi, and T. Tanabe, "Optical bistable switching action of Si high-Q photonic-crystal nanocavities," Opt. Express **13**(7), 2678–2687 (2005).